GWAs reveals SUBER GENE1-mediated suberization via Type One Phosphatases.

Jian-Pu Han[1], Linnka Lefebvre-Legendre[1], Maria Beatriz Capitão[1], Kay Gully[2], Vinay Shukla[1,3], Yibo Wu[4], Christiane Nawrath[2], Marie Barberon[1,*].

[1]Department of Plant Sciences, University of Geneva, 1211 Geneva, Switzerland
[2]Department of Plant Molecular Biology, University of Lausanne, 1015 Lausanne, Switzerland
[3]Current address: Department of Biology, University of Oxford, Oxford OX1 3RB, United Kingdom
[4]Chemical Biology Mass Spectrometry Platform, Faculty of Sciences, University of Geneva, 1211 Geneva, Switzerland
*Corresponding author

Abstract

Suberin deposition in the root endodermis is critical for plant nutrient acquisition and environmental adaptation. Here, we used an unbiased forward genetic approach based on natural variation across 284 *Arabidopsis thaliana* accessions to identify novel regulators of suberization. This screen revealed striking diversity in suberin levels and patterns, uncovering broader roles for suberin beyond those observed in the reference accession Col-0. A genome-wide association study pinpointed *SUBER GENE1* (*SBG1*), a previously uncharacterized gene encoding a 129-amino acid protein, as a key regulator of suberin deposition. SBG1 acts through physical interaction with type one protein phosphatases (TOPPs) via conserved SILK and RVxF motifs. Disrupting this interaction abolishes SBG1 function, while *topp* mutants exhibit enhanced endodermal suberization, mirroring *SBG1* overexpression. Our findings uncover a previously unknown regulatory module linking suberin formation to TOPP activity and ABA signaling and provide a framework for improving plant stress resilience through targeted manipulation of root barrier properties.

Main

Plant roots serve as the primary interface between plants and the soil, playing a critical role in nutrient acquisition and water uptake. To regulate the movement of water, ions, and nutrients, roots have evolved complex anatomical structures, including the deposition of suberin in the root endodermis. Suberin, a hydrophobic biopolymer, forms a selective barrier that not only controls radial transport but also protects plants from environmental stresses such as drought, salinity, nutrient imbalances, and pathogens[1]. The pattern of suberin deposition in the root endodermis is precisely regulated during root development[1]. In *Arabidopsis thaliana*, endodermal differentiation progresses through distinct stages. Initially, Casparian strips (CS) form an apoplastic barrier (non-suberized region) in the endodermis. Following this, patches of endodermal cells undergo suberization (patchy suberization zone), where suberin is selectively deposited. Eventually, the entire endodermal layer becomes uniformly suberized (suberized zone) (Fig. 1a). At the molecular level, the pattern of endodermal suberization is a highly regulated process, orchestrated by the interplay of several hormones and signaling pathways[1]. Abscisic acid (ABA) signaling plays a crucial role in suberin formation during development and in its induction in response to stress[2]. Additionally, CIF peptides (CASPARIAN STRIP INTEGRITY FACTOR), interacting with the Leucine-Rich Repeat Receptor-Like Kinase SGN3/GSO1 (SCHENGEN3/GASSHO1), regulate the integrity and proper function of CS by reinforcing endodermal barriers, including suberization[3,4] independently of ABA[5,6]. Recent studies have also highlighted MYB (MYELOBLASTOSIS) transcription factors, acting downstream of ABA, such as MYB9, MYB39, MYB41, MYB53, MYB92, and others[5,7-9], as key regulators controlling suberin biosynthesis, transport, and polymerization. The complexity of this regulatory network underscores suberin's central role in stress adaptation and environmental acclimation. Despite substantial progress in identifying the molecular components involved in suberin biosynthesis and regulation, no unbiased forward genetic screen has yet been conducted to discover regulators of endodermal suberization. Furthermore, natural variation in suberin deposition across plant species and genotypes remains largely unexplored.

In this study, we investigated natural variation in suberin deposition within the root endodermis. By analyzing a set of 284 *A. thaliana* accessions, we identified natural variants with distinct suberin deposition patterns and demonstrated that suberin plays a central role in mineral accumulation, extending beyond its previously established functions in the reference ecotype Col-0. Through a genome-wide association study (GWAS), we identified *SUBER GENE 1 (SBG1*), a previously uncharacterized gene encoding a 129-amino-acids protein that plays a key role in suberin regulation. We further discovered that SBG1 interacts with Type One Protein Phosphatases (TOPPs) via conserved SILK and RVxF motif, positioning it as a novel TOPPs interactor involved in fine-tuning endodermal suberization. These

findings reveal a previously unknown regulatory mechanism governing suberin formation and provide new insights into the genetic determinants of suberization and its role in plant adaptation to environmental conditions.

Results

Natural variation for endodermal suberin

To explore the variation of endodermal suberin deposition in *A. thaliana*, we analyzed the suberin pattern in 284 genetically diverse natural accessions. We stained 4-day-old seedlings with Fluorol Yellow to visualize suberin and quantified endodermal suberization by measuring the root segments that were non-suberized, patchy, or fully suberized. A wide range of suberin patterns was observed, particularly in the fully suberized zone (Fig. 1b, Supplementary Table 1). For further analysis, we selected 15 accessions with significantly less continuous suberin compared to Col-0 (referred to as "weak accessions") and 15 with significantly more continuous suberin (referred to as "strong accessions") (Fig. 1c,d). Root length is known to vary across accessions[10,11], but we found no significant correlation between the fully suberized zone and only weak correlations with the non-suberized and patchy zones (Extended Data Fig. 1a,b, Supplementary Table 1). Minor meristem size variations in specific accessions (e.g., Wei-0, Pt-0, and Lerik1-3) did not correlate with suberin patterns (Extended Data Fig. 1c). The above indicates that the observed differences in suberin pattern are not simply a consequence of differences in root growth rate. Since defects in CS formation are known to cause enhanced suberization[4,12-16], we additionally measured CS functionality using the apoplastic tracer propidium iodide (PI). We confirmed that CS functionality remained intact across the extreme accessions, ruling out defective CS formation as a driver for early or ectopic suberization (Extended Data Fig. 1d). Taken together, these data point to genetic variation directly affecting endodermal suberization, potentially linked to adaptive responses. The geographical distribution of all accessions, particularly those with extreme suberin deposition levels, was mapped, revealing a trend with strong accessions predominantly located in southern Europe, the Mediterranean region, and continental Eurasia (Extended Data Fig. 2a). To further investigate potential environmental influences, we analyzed correlations between suberin deposition and 473 climate variables (Supplementary Table 2). Several strong positive correlations were identified, including those with temperature during the warmest month, summer solar radiation, precipitation seasonality, and the global terrestrial drought index (Extended data Fig. 2b-d). Collectively, these findings are supporting the idea that the observed suberin variations are adaptive responses to local environmental factors, particularly temperature, light and water availability.

Suberin variation is associated with specific mineral imbalance

We leveraged the extreme accessions to investigate suberin function in nutrient homeostasis, a process extensively studied in Col-0[2,5,6,8]. Given that in Col-0, salt stress induces endodermal suberization and that suberin acts as barrier to limit sodium (Na) entry[2,5,17,18], we first assessed suberin induction under moderate salt stress conditions, under which Col-0 displays only a mild response (Extended Data Fig. 3a-d). In this context, all weak accessions showed an increase in suberin, though to varying degrees. Notably, Sij-4, Wei-0, and Mir-0 exhibited minimal induction, indicating a reduced sensitivity to salt-triggered suberization (Extended Data Fig. 3a,b). In contrast, most strong accessions, except Slavi-1, became fully suberized, with Shigu-1, Tsu-0, and Don-0 showing a strong reduction of the non-suberized zone, consistent with a hypersensitivity response (Extended Data Fig. 3c,d). Growth assays further revealed that several weak accessions such as Nc-1, Br-0, Sij-4, and Wei-0 maintained shoot biomass under salt stress, whereas all strong accessions, except Tsu-0 exhibited severe growth reduction (Extended Data Fig. 3e-g). These observations run counter to current models, based on Col-0 studies[2,6], that reduced suberin would confer increased salt sensitivity and enhanced suberin would provide protection.

To further explore the link between suberin variation and mineral homeostasis beyond Na, we conducted ionomic profiling of shoots from 20 extreme accessions alongside Col-0. Principal component and hierarchical clustering revealed distinct ionomic signatures between weak and strong accessions, particularly for zinc (Zn), boron (B), rubidium (Rb), copper (Cu) and molybdenum (Mo), but not Na (Fig. 1e,f, Extended Data Fig. 4a,b, Supplementary Table 3). These results highlight the pivotal role of endodermal suberization in mineral acquisition and confirm trends observed in suberin-altered Col-0 mutants and lines. Notably, B was previously shown to accumulate at lower levels in Col-0 plants with ectopic endodermal suberin and at higher levels in those with reduced suberin[5,14]. Similarly, Rb levels were reduced, while Cu and Mo levels increased in Col-0 plants with enhanced suberization[5,8,14]. However, our data also reveal differences from prior findings: Na, which typically accumulates in suberin-deficient Col-0 plants, did not vary significantly here, while Zn, lower in strong accessions in our study, has not previously been identified as a hallmark of suberin-dependent ionomic shifts. We therefore examined whether the lower Zn content observed in strong accessions might reflect an altered physiological response to Zn deficiency. Indeed, under Zn-limiting conditions, the strong accessions Sf-2 and Leo-1 displayed a more pronounced reduction in shoot biomass and developed characteristic Zn deficiency symptoms in leaves (Extended Data Fig. 4c-e). These results point to a previously underappreciated role of endodermal suberization in Zn acquisition and highlight a trade-off between protective barrier function and micronutrient uptake. While they challenge the view of suberin as a strict protective barrier against Na, our findings underscore its impact

on Zn homeostasis, revealing increased suberin deposition correlates with reduced Zn accumulation and heightened sensitivity to Zn limitation.

GWAS for endodermal suberin deposition identifies *SUBER GENE 1* (*SBG1*)

To uncover the genetic basis of natural variation in endodermal suberin deposition, we performed a Genome Wide Association Study (GWAS) for the fully suberized zone (Fig. 1b, Extended Data Fig. 5a-c, Supplementary Table 1)[19]. GWAs identified two significant loci on chromosomes 1 and 4 (Fig. 2a) with the lead SNP (*G*/*T*) on chromosome 1 located 319 bp downstream of *AT1G52565*, a previously uncharacterized gene encoding a 129 aa protein, later designated SUBER GENE1 (SBG1) (Fig. 2b). On Chromosome 4, two SNPs mapped between *AT4G05475* and *AT4G05490* encoding putative F-BOX proteins but given their greater distance from the SNPs (1839 bp and 1236 bp, respectively) (Extended Data Fig. 5d), we focused on the Chromosome 1 locus. Accessions carrying the *G* allele at this locus exhibited significantly higher suberin levels than those with the *T* allele (Extended Data Fig. 5e). To validate the role of *SBG1*, we quantified suberin deposition in available T-DNA insertion lines in Col-0 for genes within ±15 Kb of the lead SNP (Fig. 2c). Only the *sbg1-1* mutant showed significantly reduced suberin compared to WT (Fig. 2c,d, Extended Data Fig. 5f). This phenotype was independently confirmed in CRISPR-Cas9-induced *sbg1* mutants in the strong accessions Leo-1 and Tsu-0, further supporting the role of *SBG1* in suberization (Fig. 2e,f, Extended Data Fig. 5g-i). We next examined how allelic variation in *SBG1* affects suberization. Sequence analysis of *T* and *G* alleles revealed multiple additional SNPs in the 3' region (Fig. 2g). To functionally assess allele-specific effects, we cloned the genomic sequences of *SBG1*, including 1,500 bp of the 3' region, from accessions carrying either the *G* allele (Shigu-1, Sf-2 and Tsu-0) or the *T* allele (Lm-2, Nc-1 and Litva). These constructs were expressed under the constitutive and ubiquitous *UBQ10* promoter in accessions carrying the *T* allele. Constitutive expression of the *T* allele had no effect on suberization, whereas expression of the *G* alleles in weak accessions (Lm-2, Nc-1 and Litva) significantly enhanced suberization near the root tip (Fig. 2h-j). Together, these findings establish *SBG1* as a key positive regulator of suberization across natural accessions, demonstrating that allelic variations in *SBG1* modulate suberin deposition in the root endodermis.

***SBG1* is a positive regulator of endodermal suberization**

To further investigate the role of SBG1 in suberin deposition, we functionally characterized this gene in Col-0. The reduced suberin phenotype observed in *sbg1-1* (Fig. 2c,d) was confirmed with a second allele, *sbg1-2*, generated by CRISPR-Cas9 (Fig. 3a,b, Extended Data Fig. 6a). Complementation of *sbg1-1* with either SBG1 or SBG1-mVenus under its native promoter fully restored suberization (Fig. 3a,b). Furthermore, constitutive expression of SBG1-mVenus under the *UBQ10* promoter significantly enhanced suberization near the

root tip (Fig. 3c,d), mirroring the effect observed when *G* alleles were expressed in weak accessions (Fig. 2h-j). This enhanced suberization was corroborated by chemical analysis of whole root suberin content, revealing a significant increase in suberin monomers, with a 34% increase in total aliphatic content in lines constitutively expressing *SBG1* (Fig. 3e.f). These data further establish the role for *SBG1* in promoting endodermal suberin deposition.

A defining feature of genes involved in suberin formation is their specific expression in the root endodermis and their induction by ABA[2,5,7,9,20,21]. Whole-root expression analysis revealed that *SBG1* was upregulated after ABA treatment (Extended Data Fig. 6b), reaching levels comparable to *CYP86A1* (also known as *HORST, HYDROXYLASE OF ROOT SUBERIZED TISSUE*), a cognate suberin biosynthetic enzyme. To refine this expression pattern, we generated *SBG1::NLS-3xmVenus* transcriptional reporter lines. Promoter activity was initially detected in the columella and early endodermal lineage cells at the root tip (Fig. 3g). In differentiated roots, *SBG1* promoter activity was observed primarily in the endodermis and to a lower extent in vascular tissues (Fig. 3g). Consistent with suberin-related genes such as *MYB41, MYB92,* and *GPAT5*[2,5]*, SBG1* promoter activity was further enhanced by ABA treatment, expanding toward the meristematic zone (Fig. 3h). The A. thaliana genome contains three uncharacterized homologs of *SBG1* (hereafter named *SBG1-Like1, 2* and *3* or *SBG1L1*, *SBG1L2* and *SBG1L3*) (Extended Data Fig. 6c). The quadruple *sbg1;sbg1l1;sbg1l2;sbg1l3* (*quad-sbg1*) mutant exhibited a stronger reduction in suberin deposition compared to the single *sbg1* mutant (Fig. 3i,j, Extended Data Fig. 6d). More strikingly, ABA-induced suberin deposition was progressively reduced in *sbg1, sbg1;sbg1l1,* and *quad-sbg1* mutants, suggesting that SBG1 and its homologs fine-tune ABA response in the endodermis (Fig. 3i,j). Together, these results establish SBG1 as a positive regulator of endodermal suberization, possibly contributing to ABA-mediated suberin deposition. However, given that *SBG1* encodes a small 129-amino-acid protein with no known functional domains, its precise role in suberin formation remains elusive (Extended Data Fig. 7a).

SBG1 promotes suberization through interaction with TOPPs

Given that SBG1 is a small protein of only 129 amino acids, we hypothesized that its molecular function might be regulatory, mediated through protein-protein interactions. We first assessed SBG1 subcellular localization with SBG1-mVenus and SBG1-mCherry fusion proteins, which exhibited a reticulated signal colocalizing with an ER marker (Fig. 4a, Extended Data Fig. 7b). We next performed immunoprecipitation (IP) of SBG1-mVenus from plants constitutively expressing the fusion protein, followed by mass spectrometry (MS) analysis. Enriched proteins were identified by comparison with an IP control from plants expressing ER-GFP. Among the most highly enriched proteins (Supplementary Table 4), we

identified 2 Type One Protein Phosphatases (TOPPs): TOPP2 and TOPP1(Extended Data Fig. 7c). Notably, we also detected enrichment of TOPP7, TOPP8, TOPP4, and TOPP5, meaning that 6 out of the 9 TOPPs present in A. thaliana were enriched in the SBG1 IP-MS dataset (Extended Data Fig. 7c).

TOPPs are a family of serine/threonine phosphatases with broad functions in plants, including cell division, differentiation, salt tolerance and ABA signaling[22]. They are orthologs of Protein Phosphatase 1 (PP1) in animals and fungi, where their activity is modulated by regulatory subunits that interact through conserved RVxF and SILK motifs[23]. These regulatory interactions can either inhibit TOPPs activity by blocking substrate access (as seen for Inhibitor-2, I2) or recruit substrates while controlling access to the catalytic site (as observed for Kinetochore Null Protein 1, KNL1)[22,24,25]. Strikingly, SBG1 and SBG1L1 contain a SILK motif, while all 4 SBG1 homologs (SBG1, SBG1L1, SBG1L2, and SBG1L3) harbor an RVxF motif, suggesting a potential role in TOPP regulation (Extended Data Fig. 6c). To assess this possibility, we first employed an in-silico structural approach using AlphaFold3[26], focusing on TOPP2, the most enriched phosphatase in our IP-MS dataset. Predicted local distance difference test (plDDT) showed high confident prediction with interface predicted template modeling (ipTM) of 0.85 and predicted template modeling (pTM) of 0.79, comparable to those observed for the well-characterized interactions between TOPP and I2 in A. thaliana[25,27] (Fig. 4b, Extended Data Fig. 7d-f). In this analysis, SBG1 is predicted to interact with TOPP2 via its central region, which contains both SILK and RVxF motifs (Fig. 4b, Extended Data Fig. 7d,e). Notably, a similar interaction is predicted for SBG1L1, which also harbors both motifs (Extended Data Fig. 6c and 7f). In contrast, SBG1L2 and SBG1L3 contain only the RVxF motif, and their predicted interactions with TOPP2 only partially overlap with that of SBG1 (Extended Data Fig. 6c and 7f). Additionally, the C-termini of SBG1 homologs and the known TOPP inhibitor I2 are predicted to form similar structural covering over the TOPP2 catalytic site. This is particularly evident for SBG1 and SBG1L1, which possess extended C- terminal loops (Extended Data Fig. 7f), suggesting that SBG1 proteins may inhibit TOPP2 activity by sterically blocking access to its catalytic site. We next experimentally validated this interaction using a yeast two-hybrid assay confirming SBG1 interaction with TOPP1 and TOPP2 and the requirement of both SILK and RVxF motifs for SBG1 interaction with TOPP1 and TOPP2 (Fig. 4c,d).

To our knowledge, TOPPs have not previously been implicated in suberin or polyester formation. However, previous studies showed that *topp* loss-of-function mutants are hypersensitive to ABA, and TOPP1 was reported to inactivate SNF1-related protein kinase 2.6 (SnRK2.6, also known as Open stomata, OST1), a key positive regulator of ABA signalling[27,28]. Consistently, we observed that SBG1-mVenus overexpressing lines, but not

sbg1 mutants, displayed ABA hypersensitivity comparable to previously described *topp* mutants (Extended Data Fig. 7g,h)[28]. This suggests that SBG1 may inhibit TOPP activity, thereby modulating ABA signaling. We next examined suberin deposition in *topp* mutants and found a significant increase in suberin levels with ectopic deposition near the root tip in the mutant *topp2*, a phenotype resembling *UBQ10::SBG1-mVenus* overexpression lines and opposite to that of *sbg1* mutants (Fig. 4e, Extended Data Fig. 7i). This could indicate that SBG1 promotes suberization by antagonizing TOPP2 function in ABA signaling. Fitting with this hypothesis, *TOPP2* promoter is active in the endodermis similar to *SBG1* (Fig. 4f). To directly test this model, we generated mutagenized SBG1-mVenus constructs lacking a functional RVxF motif or both SILK and RVxF motifs and expressed them constitutively. Unlike the WT SBG1-mVenus construct, both mutants failed to induce suberin deposition (Fig. 4g,h). This confirms that SBG1's positive role in suberization is mediated through its interaction with TOPPs. Together, these results establish SBG1 as a key regulator of suberization, acting through inhibition of TOPP phosphatases, possibly by restricting their catalytic activity via direct protein-protein interaction.

Discussion

Suberin deposition in roots has attracted growing attention due to its role as a protective barrier against drought and pathogens and as a potential contributor to underground carbon storage. In particular, suberization of the endodermis and exodermis forms a dynamic barrier for water and nutrients[2,6,29-34]. Key regulators of endodermal suberin deposition are conserved across vascular plants and were instrumental in the evolution of seed plants[31,35-37]. While substantial progress has been made in understanding the molecular pathway of suberin biosynthesis and regulation, most insights come from the *A. thaliana* reference accession Col-0. Moreover, no unbiased, forward genetic approach, aiming at identifying unknown players in suberization had been performed. Previous studies on natural variation in suberin have focused on peridermal suberization in older roots[38], linking chemical diversity in suberin to soil properties and moisture gradients, identifying 94 putative loci, with verification for *GPAT6*, which has a demonstrated role in suberin biosynthesis[20,38]. Here, we targeted the genetic diversity underlying the highly plastic endodermal suberization to uncover mechanisms involved in nutrient acquisition and stress adaptation. Our screen revealed a strong association between endodermal suberization and accumulation of Rb, Mo, Cu and Zn in shoots. Unexpectedly, K and Na, classical markers of endodermal suberin levels in Col-0, were not affected, emphasizing that Col-0 may not be representative of species-wide responses, particularly for traits linked to root developmental physiology, as shown before for Zn and P deficiencies responses and for root growth response to hormones[39,40]. While previous studies in Col-0 linked endodermal suberin to B, Rb, Cu and Mo accumulation[5,8,14], a consistent impact on Zn was not shown before. Accessions with

enhanced suberin accumulated less Zn, showed increase sensitivity to Zn deficiency, mirroring earlier findings that Zn limitation downregulated suberization, likely to facilitate Zn uptake[2]. Together, these results position endodermal suberin as a key regulator of Zn homeostasis, with implications for nutrient adaptation strategies in plants.

Our GWAs analysis identified multiple loci associated with endodermal suberization, including two that surpassed the Bonferroni-corrected significance threshold and more than 20 additional loci exceeding the Benjamini–Hochberg threshold. Strikingly, none of the previously known regulators of suberin deposition were found among these loci, underscoring the strength of this unbiased approach in uncovering novel genetic determinants. Focusing on the strongest association on chromosome 1, we identified *SBG1*, a previously unannotated gene whose naturally occurring allelic variation impacts the pattern of suberin deposition across accessions, suggesting a major role in suberin-dependent environmental adaptation. Supporting a direct role in suberization, *SBG1* is expressed in the endodermis and is transcriptionally induced by ABA, a well-established hormonal regulator of endodermal suberin deposition, during both stress responses and root development[2,5,6,35]. Consistent with its expression pattern, *SBG1* regulates ABA-induced endodermal suberization and physically interacts with the protein phosphatases TOPPs, particularly TOPP2, which is constitutively expressed in the endodermis. Since TOPPs are known negative regulators of ABA signaling[27,28], our findings suggest that SBG1 interferes with TOPP activity, thereby locally relieving ABA repression and promoting suberin formation. The enhanced suberin phenotype observed in the *topp2* mutant, which phenocopies *SBG1* constitutive expression, further supports TOPP2 as a central target of SBG1-mediated suberin regulation. Together, our results define a novel regulatory module that fine-tunes ABA signaling in the endodermis to control suberin deposition. Given the evolutionary conservation of SBG1 across angiosperms (Extended Data Fig. 8a,b), this mechanism likely represents a fundamental and broadly relevant strategy for regulating root barrier properties in diverse plant species.

Together, our findings highlight the power of unbiased forward genetic approaches to uncover previously unknown regulators of endodermal suberin deposition. By revealing the genetic basis underlying natural variation in suberin deposition, we identify SBG1 as a central, previously uncharacterized regulator of this key traits. This work not only advances our understanding of the mechanisms governing root barrier formation but also provides a new conceptual and molecular framework to manipulate suberin deposition for improving plant stress resilience.

Material and methods

Plant material

The 284 Arabidopsis accessions used in this study are listed in Supplementary Table 1. These accessions represent a subset of the 1001 Genomes Project[41], including 185 of the 195 Salk accessions, 80 Max-Planck Institute accessions, and the 19 founder accessions used to generate the MAGIC (Multiparent Advanced Generation Inter-Cross) population[42]. The ER-GFP marker line was described previously[43]. The T-DNA insertion lines *sbg1-1* (SALK_029983C), *frs6-2* (SALK_114017C)[44], *at1g52540* (GK-090F10), *at1g52550* (SAIL_681_G01), *pldα2* (GK-212E06), *rbl5* (SALK_079189C), *at1g52590* (SAIL_894_H03.C), *at1g52600* (SALK_062346C), *topp1* (SALK_057537)[27,45], *topp2* (GK-187C10)[28], *topp6* (SALK_093747C)[45], *topp7* (SALK_023073C)[45], *topp8/aun2-1* (SALK_137888)[46] and *topp9/aun1-1* (SALK_045433C)[45,46] were obtained from the Nottingham Arabidopsis Stock Centre, and genotyping primers are provided in Supplementary Table 5. Additional mutants (*sbg1-2, sbg1-3, sbg1-4, sbg1;sbg1l1 and quad-sbg1*) were generated via CRISPR-Cas9 in specified accessions using guide RNAs described in the Constructs section. The following transgenic lines were developed in this study: *UBQ10::SBG1_acc* (*SBG1* from specified accessions), *UBQ10::SBG1-mVenus*, *UBQ10::SBG1_SM-mVenus, UBQ10::SBG1_DM-mVenus, SBG1::NLS-3xmVenus*, *SBG1::SBG1*, *SBG1::SBG1-mVenus, UBQ10::SBG1-mCherry* and *TOPP2::NLS-3xmvenus*. The corresponding gene IDs are: *SBG1*, *AT1G52565*; *SBG1L1*, *AT3G15760*; *SBG1L2*, *AT2G35850*; *SBG1L3*, *AT3G52360*; *TOPP1*, *AT2G29400*; *TOPP2*, *AT5G59160*; *TOPP6*, *AT5G43380*; *TOPP7*, *AT4G11240*; *TOPP8*, *AT5G27840*; *TOPP9*, *AT3G05580*; *GPAT5*, *AT3G11430*; *CYP86A1*, *AT5G58860*; *MYB41, AT4G28110*; *FRS6, AT1G52520*; *PLDα2, AT1G52570*; *RBL5, AT1G52580*; *I2, AT5G52200*.

Constructs and plant transformation

CRISPR-Cas9 constructs targeting *SBG1* were designed using Benchling (https://www.benchling.com/) (Supplementary Table 5). Oligonucleotides for guide RNAs were annealed, digested by BbsI, and ligated into the pEN-Chimera vector[47]. The resulting entry constructs were recombined using the Gateway Technology® (Thermo Fisher Scientific) into a destination vector containing the *UBQ10::SpCas9* and a FAST Red selection marker[48]. Entry clones for expression constructs were generated using Gibson assembly following PCR amplification. PCR products were cloned into a BamHI-digested pUC57-L4_EcoRV-XbaI-BamHI_R1 or into a NotI-digested pDONR221-*L1_SpeI-BglII-NotI-SphI-EcoRI_L2*. Newly generated entry clones are: *L4-proSBG1-R1* (3000bp promoter), *L4-proTOPP2-R1* (1322bp), *L1-SBG1-L2* (genomic *SBG1* without stop codon from Col-0), *L1-SBG1_acc-L2* (genomic *SBG1* including 1500 bp of 3' region from specified accession). *L1-SBG1_SM-L2* and *L1-SBG1_DM-L2*_were synthesized and then recombined in the same way as for *UBQ10::SBG1-mVenus*. For yeast two-hybrid assay, CDS of *SBG1* 88-390bp, *TOPP1*

and *TOPP2* were cloned in pDONR221 by Gateway BP reaction. *L1-SBG1_SM (V63A/F65A)-L2* and *L1-SBG1_DM (V63A/F65A, C46A/L47A)-L2* 88-390bp were synthesized. Then they were recombined into pGADT7 or pGBKT7 (TaKaRa) by Gateway LR reaction. Previously described entry clones include *L4-pUBQ10-R1*[49] (promoter), *L1-nls-3xmVenus-L2*[50], *R2-mCherry-L3*[50], *R2-mVenus-L3*[51] and *R2-mScarletI-L3*[52] (CDS), and *R2-tHSP18.2-L3*[53] and *R2-tNOS-L3*[54] (terminators). Expression clones were generated using the Multisite Gateway Technology (Life Technologies, Carlsbad, CA, USA) by recombination of entry clones into the destination vectors pFR7m34GW (FAST Red) or pFG7m34GW (FAST Green)[53]. Primers used for cloning are listed in Supplementary Table 5. Final constructs were introduced into Arabidopsis using *Agrobacterium tumefaciens* strain GV3101 and the floral dip method[55]. For each construct, at least 14 T1 seeds were selected based on fluorescence (FAST Red or FAST Green)[56]. Segregation ratios, gene expression levels, and phenotypes were analyzed across 14 independent T2 lines. All experiments were conducted on T3 homozygous lines with mono-insertional events unless otherwise noted.

Growth conditions

For *in vitro* experiments, seeds were surface sterilized using chlorine gas and sown on square plates. Unless stated otherwise, seedlings were grown on half-strength MS (Murashige and Skoog) medium (pH 5.7) containing 0.8 % agar without sucrose. For nutrient deficiency assays, the medium was prepared using a 20x macronutrient stock solution (Sigma-Aldrich, M0654), 2000x individual micronutrient stock solutions consisting to reach a final concentration of 9.4 mM KNO_3, 10.3 mM NH_4NO_3, 625 mM KH_2PO_4, 1.49 mM $CaCl_2$, 0.75 mM $MgSO_4$, 50 µM H_3BO_3, 0.05 µM $CuSO_4 \cdot 5 H_2O$, 50 µM $MnSO_4 \cdot H_2O$, 0.5 µM $Na_2MoO_4 \cdot 2 H_2O$, 15 µM $ZnSO_4 \cdot 7 H_2O$, 2.5 µM KI, 0.05 µM $CoCl_2 \cdot 6 H_2O$, 50 µM Fe-EDTA. MES (0.5 g/L) was added and pH adjusted to 5.7 with KOH. For nutrient-deficient conditions, the specified nutrient was omitted from the medium. For the suberin screening in 284 accessions, seeds were stratified for 7 days at 4°C to minimize germination variability. For other experiments, stratification was performed for 2 to 3 days at 4°C. Seedlings were grown vertically in growth cabinets set to 22°C under continuous light (~100 µE) and 40% relative humidity. For propagation, plants were grown under long-day conditions (16 h light/8 h dark) at 20 ± 2°C, with a light intensity of 150-180 µE and 60% relative humidity. Experiments were conducted on 5-day-old seedlings unless otherwise specified.

Suberin staining and pattern quantification

For suberin histological analysis, seedlings were whole mount stained as described previously[5]. Briefly, whole seedlings were immersed in Fluorol Yellow 088 (0.01% w/v, lactic acid; Chem Cruz, Cat# sc-215052) and incubated at 70°C for 30 minutes in the dark. After staining, seedlings were washed twice with water and counterstained with aniline blue (0.5%

w/v; Sigma-Aldrich, Cat# 415049) for 30 minutes at room temperature in the dark, followed by two additional water washes. For imaging, seedlings were mounted on slides in 50% glycerol and scanned using a ZEISS Axio Zoom.V16 stereomicroscope equipped with a GFP filter (excitation: 450-490 nm, emission: 500-550 nm). Full root imaging at high resolution was achieved using a tile-scanning approach. The region of interest (ROI) was first defined during a low-resolution scan (7x magnification). Focus points were manually selected along the root to ensure consistent focus, and high -resolution images (63x magnification) were captured as overlapping tiles (10% overlap) that were subsequently stitched together. Suberin pattern quantification was performed by measuring the lengths of three distinct suberin zones along the root (non-suberized, patchy, and fully suberized) using Fiji[57] software as previously described[5].

Correlations of suberin pattern with climate factors

Climate data for the Arabidopsis accessions analyzed in this study were retrieved from AraCLIM (https://github.com/CLIMtools/AraCLIM)[58]. Relevant climate variables were selected and extracted for the geographic origin of the characterized accessions. Correlations between suberin quantification and environmental variables were performed using non-parametric Spearman correlation analysis in GraphPad Prism 10 (https://www.graphpad.com/).

Propidium iodide staining and uptake assay

Propidium iodide (PI) was used to counterstain cell walls and as an apoplastic tracer for evaluating Casparian strips functionality, as described previously[59]. Seedlings were live stained with 15 µM PI in darkness for 10 minutes, followed by two washes with water. For the PI uptake assay, the functionality of the apoplastic barrier was assessed by counting the number of endodermal cells beyond the onset of elongation where PI uptake was blocked by Casparian strips. The onset of elongation was defined as the point where the first endodermal cell exhibited a length at least three times its width. Observations were made using a Leica DM6 B epifluorescence microscope equipped with an I3 filter at 20x magnification.

Confocal microscopy and image analysis

Confocal microscopy imaging was performed using Leica SP8, Zeiss LSM 780, and Zeiss LSM 800 microscopes. Excitation and detection wavelengths were set as follows: for Leica SP8 system, GFP/mVenus (488 nm, 500-546 nm), PI/mCherry (552 nm, 585-617 nm); for Zeiss LSM 800, GFP/mVenus (488 nm, 500-546 nm), PI (561 nm, 585-617 nm); for Zeiss LSM 780 mVenus (514 nm, 515-561 nm), PI (514 nm, 585-679 nm). Scanner and detector settings were maintained constantly across all experiments to ensure consistency. Image analyzed

was conducted using ZEN2.3 software (ZEISS) and Fiji[57] (http://fiji.sc/Fiji).

Ionomic analysis

Elemental content in 7-day-old leaves was measured using Inductively Coupled Plasma Mass Spectrometry (ICP-MS). Dried leaves were weighed and transferred to 15 mL metal-free Falcon tubes (VMR). Samples were digested with 300 µL of 67% nitric acid (Fisher Chemicals) containing 100 ppb indium as an internal standard and incubated in a dry block heater at 100˚°C for 2 hours. After cooling, digests were diluted to 15 mL with Milli-Q water (Merck Millipore). Elemental analysis was performed on an Agilent 7700X ICP-MS with an autosampler operating in helium collision mode. Scandium (2 ppb) was added as an on-site internal standard. Fifteen elements (B, Na, Mg, P, S, K, Ca, Mn, Fe, Co, Cu, Zn, Rb, Sr and Mo) were monitored. Calibration standards were prepared using single-element standards solutions (Inorganic Ventures; Suisse Technology Partners Ltd.). A standard reference material (NIST1515, apple leaves, Sigma-Aldrich) was included to validate analytical methods. Element concentrations in the samples were calculated using the external calibration method, normalized to the dry weight, and processed with the instrument software.

Suberin monomer analysis

Suberin monomers analysis in roots was conducted by gas chromatography-mass spectrometry (GC-MS) following a previously described protocol[60]. Roots from 5-day-old seedlings (200-300 per replicate) were harvested and incubated in isopropanol containing 0.01% butylated hydroxytoluene (BHT) at 85°C for 10 minutes. Delipidization was performed twice (16 hours and 8 hours) using extractions with chloroform-methanol (2:1), chloroform-methanol (1:1), and methanol with 0.01% BHT, with samples continuously agitated. The delipidized samples were vacuum-dried for 3 days before depolymerization via base catalysis. For depolymerization, dried plant material was subjected to trans-esterified in a reaction medium (20 mL) composed of 3 mL methyl acetate, 5 mL of 25% sodium methoxide in dry methanol, and 12 mL dry methanol. Methyl heptadecanoate (5 mg) and ω-pentadecalactone (10 mg) were added as internal standards per sample. The samples were incubated at 60°C for 2 hours, followed by the addition of 3.5 mL dichloromethane, 0.7 mL glacial acetic acid, and 1 mL 0.9% NaCl in 100 mM Tris-HCl buffer (pH 8.0). Samples were vortexed for 20 seconds and centrifuged at 1500 x g for 2 minutes. The organic phase was collected, washed with 2 mL 0.9% NaCl, dried over sodium sulfate, and concentrated under a nitrogen stream. The suberin monomers were derivatized with N,O-bis(trimethylsilyl)trifluoroacetamide (BFTSA) in pyridine (1:1, v/v) at 70°C for 1 hour before GC-MS analysis. Samples were injected in hexane onto an HP-5MS column (J&W Scientific) using an Agilent 6890N GC Network systems coupled to a mass spectrometer and flame

ionization detector. The oven temperature was programmed as follows: 50°C for 2 minutes, an increase of 20°C/min to 160°C, 2 °C/min to 250°C, and 10°C/min to 310°C, held for 15 minutes. The amounts of unsubstituted C16 and C18 fatty acids were excluded from the analysis due to their widespread occurrence in plants and the environment.

Genome-wide association analysis

The GWAS was performed on GWA-Portal (https://gwas.gmi.oeaw.ac.at/) with the data of the fully suberized zone quantified in 265 accessions (Supplementary Table 1) and Imputed Full sequence Dataset corresponding of a combination of the 250K SNP dataset and the 1001 genomes dataset using imputation (TAIR9)[61]. An accelerated mixed model (AMM) was applied for the GWAS and a significance threshold of 10% was used after Bonferroni-Hochberg correction for multiple tests.

Protein sequence alignment and phylogenetic analysis

The protein sequences of SBG1, SBG1L1, SBGL2 and SBG1L3 were aligned with Clustal Omega methods on SnapGene (https://www.snapgene.com/). The protein sequences of SBG1 orthologs were acquired by NCBI's protein blast to select the protein with the highest similarity across different species. Sequences were subsequently aligned with the Clustal Omega methods in (https://www.ebi.ac.uk/jdispatcher/msa/clustalo)[62]. The phylogenetic analysis was conducted on ClustalW2 with Phylip output format and Neighbour-joining clustering methods (https://www.ebi.ac.uk/jdispatcher/phylogeny/simple_phylogeny)[62].

qRT-PCR

Gene expression analyses were performed using roots from 7-day-old seedlings, with approximately 60 roots pooled per biological replicate (3 biological replicates per genotype and conditions). After harvesting, roots were immediately frozen in liquid nitrogen and subsequently ground to a fine powder using a tissue lyser. Total RNA was extracted using the TRIzol reagent (Ambion) and further purified with the RNeasy MinElute Cleanup Kit (Qiagen). Reverse transcription was performed with the Maxima First Strand cDNA Synthesis Kit (Thermo Scientific). Quantitative real-time PCR (qRT-PCR) was conducted on an Applied Biosystems QuantStudio5 thermocycler using SYBR Green master mix (Applied Biosystems). The expression levels were normalized to the housekeeping gene *Clathrin AP4M* (*AT4G24550*), and relative expression was calculated using the $2^{-\Delta\Delta Ct}$ method[63]. Primers used for qRT-PCR are detailed in Supplementary Table 5.

IP-MS analysis

Roots of 7-day-old seedlings expressing SBG1-mVenus and ER-GFP were harvested for protein extraction. After grinding the total protein was extracted with 50 mM Tris-HCl pH 7.5,

150 mM NaCl, 2 mM EDTA, 5 mM Dithiothreitol, 1 mM PMSF, 1% Triton X-100 and protease inhibitor cocktail (Roche). To immunoprecipitate mVenus- or GFP-tagged proteins, GFP-Trap Magnetic Agarose beads (Chromotek) were added to the supernatant of protein extracts. Beads were first washed 3 times with 50 mM Tris-HCl pH 7.5, 150 mM NaCl, 2 mM EDTA, 0.01% Triton X-100, then 3 more times with 50 mM Tris-HCl pH 7.5, 150 mM NaCl. The beads were kept in the second washing buffer. To prepare samples for proteomic analysis, the remaining buffer was removed, and the beads were suspended in 100 µL 1 M Urea in 50 mM Ammonium bicarbonate. Samples were reduced using a final concentration of 10 mM DTT at RT for 30 min and alkylated with 20 mM iodoacetamide at RT for 30 min in the dark. Alkylation reactions were quenched with a half amount of DTT used for the reduction and incubated 10 min at RT in the dark. Finally, beads were incubated with 300 ng Trypsin (Promega, USA) in 1 mM hydrochloric acid and 25 mM ammonium bicarbonate and digested overnight at 25°C. Afterward, digestion was stopped by adding 10% TFA to reach a final concentration of 0.5%, centrifuged and deposited on a magnetic rack to transfer the supernatant into a fresh tube. Tryptic peptides were desalted using MonoSpin C18 columns (GL Sciences Inc., Japan) and eluted from C18 columns using 0.1% TFA in 50% acetonitrile and dried in a centrifugal vacuum concentrator. Tryptic peptides were dissolved in 0.1% (v/v) formic acid in 2% (v/v) acetonitrile for mass spectrometry (MS) analysis.

For MS analysis, samples were measured on an Easy Nano LC Orbitrap Fusion System equipped with a nanospray flex™ ion source (Thermo Fisher Scientific, USA). Peptides were separated on a 1.9 µm particle, 75 µm inner diameter, 15 to 20 cm filling length homemade C18 column. A flow rate of 300 nL/min was used with a 2 h gradient 3–30% solvent B. The gradient followed with two rounds of washing steps, in each step, the gradient switched to 90% solvent B in 1 min and kept for another 5 min, and switched to 3% solvent B in 1 min and kept for another 5 min. In the second round of washing the 90% B solvent was kept for 2 min, an extra 14 min of 3% solvent B was kept for system equilibration. Solvent A was 0.1% (v/v) formic acid in LC/MS grade water and solvent B was 0.1% (v/v) formic acid in 100% (v/v) acetonitrile. The ion source settings from Tune were used for the mass spectrometer ion source properties.

For data-independent acquisition (DIA), data were acquired with 1 full MS and 41 overlapping isolation windows constructed covering the precursor mass range of 350–1400 m/z. For full MS, Orbitrap resolution was set to 120,000. Automatic Gain Control (AGC) target was set to custom with normalized AGC target set to 50%, and maximum injection time (IT) was set to 100 ms. DIA segments were acquired at a resolution of 30,000. AGC target was set to custom with normalized AGC target set to 200%, and a 54 ms maximum IT. HCD fragmentation was set to normalized collision energy of 28%. For protein identification and quantification, Raw files from DIA measurements were analyzed using the directDIA workflow in Spectronaut software (Biognosys, Switzerland) with default settings.

Identification was performed using the Uniprot reference proteome UP000006548 for Arabidopsis thaliana.

Alphafold3 analysis

Protein interaction between SBG1, SBG1L1, SBG1L2, SG1L3, I2 and TOPP2 was predicted by AlphaFold3 model (https://alphafoldserver.com/). Full protein sequences of SBG1s, I2, TOPP2 and 2x Mn^{2+} were entered as input for the prediction. pLDDT coded structure and PAE plots indicating the quality of the prediction are shown in Extended Data Fig. 7 d,e. Final models were imported and modified with PyMOL V3.1.0 (https://www.pymol.org/).

Yeast two-hybrid

Yeast two-hybrid analyses were conducted using Matchmaker Gold Yeast Two-Hybrid System (Clontech; TaKaRa, Tokyo, Japan) according to the manufacturer's protocols. Yeast strain (Y2HGold) was co-transformed with the respective AD and BD plasmids and transformants were selected on SD-LW (leucine, tryptophane). For interaction analysis, 5µl of yeast culture dilutions in the indicated concentration range were spotted on both SD-LW and SD-LWH (leucine, tryptophane, histidine) plates and incubated at 28°C for 3 d.

Statistical analysis

Statistical analysis and graph generation were performed using GraphPad Prism 10 (https://www.graphpad.com/). All experiments were conducted independently at least 3 times, yielding consistent results, except for the proteomic analysis (2 independent experiments with 3 biological replicates). All the datasets were first tested for normal distribution and equality of variances before subjecting for parametric or non-parametric test accordingly. The tests used are specified in the legends. The PCA and clustering analysis of ionomic profiles were performed on MVApp[64] (https://mvapp.kaust.edu.sa/).

Acknowledgments

We are grateful to Robertas Ursache, Lothar Kalmbach and Satoshi Fujita for sharing plasmids. We thank Sylvain Loubéry and the Photonic Bioimaging Center at the University of Geneva for their invaluable assistance with microscopy and image analysis, as well as Sophie Michalet and the ICP-MS center at University of Geneva for support with ionomic analyses. We thank Jun Yu and Houming Chen for their support on IP-MS analysis and AlphaFold predictions. We also acknowledge Mylène Docquier and the iGE3 (Institute of Genetics and Genomics in Geneva) platform for their contribution to RNA sequencing and data analysis. We thank Richard Chappuis and Roman Ulm for their guidance with yeast two-hybrid. Special thanks go to Laura Peréz Martín, Fabienne Cléard-Karch, Léa Jacquier,

and Kevin Robe for their assistance with sample collection for chemical analyses of suberin. Isabelle Fleury is warmly thanked for her dedicated support in plant growth and propagation. This work was supported by the Sandoz Family Monique De Meuron philanthropic foundation's program for academic promotion and the Swiss National Science Foundation (PCEGP3_187007) awardee to MB, as well as by the state of Geneva.

References

1 Shukla, V. & Barberon, M. Building and breaking of a barrier: Suberin plasticity and function in the endodermis. *Current Opinion in Plant Biology* **64**, 102153 (2021). https://doi.org/10.1016/j.pbi.2021.102153

2 Barberon, M. *et al.* Adaptation of Root Function by Nutrient-Induced Plasticity of Endodermal Differentiation. *Cell* **164**, 447-459 (2016). https://doi.org/10.1016/j.cell.2015.12.021

3 Doblas, V. G. *et al.* Root diffusion barrier control by a vasculature-derived peptide binding to the SGN3 receptor. *Science* **355**, 280-284 (2017).

4 Pfister, A. *et al.* A receptor-like kinase mutant with absent endodermal diffusion barrier displays selective nutrient homeostasis defects. *Elife* **3** (2014).

5 Shukla, V. *et al.* Suberin plasticity to developmental and exogenous cues is regulated by a set of MYB transcription factors. *Proceedings of the National Academy of Sciences* **118** (2021). https://doi.org/10.1073/pnas.2101730118

6 Wang, P. *et al.* Surveillance of cell wall diffusion barrier integrity modulates water and solute transport in plants. *Scientific reports* **9**, 4227 (2019). https://doi.org/10.1038/s41598-019-40588-5

7 Kosma, D. K. *et al.* AtMYB41 activates ectopic suberin synthesis and assembly in multiple plant species and cell types. *The Plant Journal* **80**, 216-229 (2014).

8 Cohen, H., Fedyuk, V., Wang, C., Wu, S. & Aharoni, A. SUBERMAN Regulates Developmental Suberization of the Arabidopsis Root Endodermis. *The Plant Journal* **102**, 431-447 (2020). https://doi.org/10.1111/tpj.14711

9 Xu, H. *et al.* Transcriptional networks regulating suberin and lignin in endodermis link development and ABA response. *Plant Physiol* **190**, 1165-1181 (2022). https://doi.org/10.1093/plphys/kiac298

10 Mouchel, C. F., Briggs, G. C. & Hardtke, C. S. Natural genetic variation in Arabidopsis identifies BREVIS RADIX, a novel regulator of cell proliferation and elongation in the root. *Genes & Development* **18**, 700-714 (2004). https://doi.org/10.1101/gad.1187704

11 Meijón, M., Satbhai, S. B., Tsuchimatsu, T. & Busch, W. Genome-wide association study using cellular traits identifies a new regulator of root development in Arabidopsis. *Nature Genetics* **46**, 77-81 (2014). https://doi.org/10.1038/ng.2824

12 Hosmani, P. S. *et al.* Dirigent domain-containing protein is part of the machinery required for formation of the lignin-based Casparian strip in the root. *Proceedings of the National Academy of Sciences* **110**, 14498-14503 (2013).

13 Kalmbach, L. *et al.* Transient cell-specific EXO70A1 activity in the CASP domain and Casparian strip localization. *Nature Plants* **3**, 17058 (2017). https://doi.org/10.1038/nplants.2017.58

14 Kamiya, T. *et al.* The MYB36 transcription factor orchestrates Casparian strip formation. *Proceedings of the National Academy of Sciences* **112**, 10533-10538 (2015). https://doi.org/10.1073/pnas.1507691112

15 Li, B. *et al.* Role of LOTR1 in Nutrient Transport through Organization of Spatial Distribution of Root Endodermal Barriers. *Current Biology* **27**, 758-765 (2017).

16 Gao, Y.-Q. *et al.* A dirigent protein complex directs lignin polymerization and assembly of the root diffusion barrier. *Science* **382**, 464-471 (2023). https://doi.org/doi:10.1126/science.adi5032

17 Ursache, R. *et al.* GDSL-domain proteins have key roles in suberin polymerization and degradation. *Nature Plants* **7**, 353-364 (2021). https://doi.org/10.1038/s41477-021-00862-9

18 Krishnamurthy, P., Vishal, B., Bhal, A. & Kumar, P. P. WRKY9 transcription factor regulates cytochrome P450 genes and , leading to increased root suberin and salt tolerance in Arabidopsis. *Physiologia Plantarum* **172**, 1673-1687 (2021). https://doi.org/https://doi.org/10.1111/ppl.13371

19 Seren, Ü. in *Root Development: Methods and Protocols* (eds Daniela Ristova & Elke Barbez) 303-319 (Springer New York, 2018).

20 Gully, K. *et al.* The GPAT4/6/8 clade functions in Arabidopsis root suberization nonredundantly with the GPAT5/7 clade required for suberin lamellae. *Proceedings of the National Academy of Sciences* **121**, e2314570121 (2024). https://doi.org/10.1073/pnas.2314570121

21 Yadav, V. *et al.* ABCG Transporters Are Required for Suberin and Pollen Wall Extracellular Barriers in Arabidopsis. *The Plant Cell* **26**, 3569-3588 (2014).

22 Uhrig, R. G., Labandera, A. M. & Moorhead, G. B. Arabidopsis PPP family of serine/threonine protein phosphatases: many targets but few engines. *Trends in Plant Science* **18**, 505-513 (2013). https://doi.org/10.1016/j.tplants.2013.05.004

23 Srivastava, G., Choy, M. S., Bolik-Coulon, N., Page, R. & Peti, W. Inhibitor-3 inhibits Protein Phosphatase 1 via a metal binding dynamic protein–protein interaction. *Nature Communications* **14**, 1798 (2023). https://doi.org/10.1038/s41467-023-37372-5

24 He, Y. *et al.* Arabidopsis KNL1 recruits type one protein phosphatase to kinetochores to silence the spindle assembly checkpoint. *Sci Adv* **11**, eadq4033 (2025). https://doi.org/10.1126/sciadv.adq4033

25 Templeton, George W. *et al.* Identification and characterization of AtI-2, an Arabidopsis homologue of an ancient protein phosphatase 1 (PP1) regulatory subunit. *Biochemical Journal* **435**, 73-83 (2011). https://doi.org/10.1042/bj20101035

26 Abramson, J. *et al.* Accurate structure prediction of biomolecular interactions with AlphaFold 3. *Nature* **630**, 493-500 (2024). https://doi.org/10.1038/s41586-024-07487-w

27 Hou, Y.-J. *et al.* Type One Protein Phosphatase 1 and Its Regulatory Protein Inhibitor 2 Negatively Regulate ABA Signaling. *PLOS Genetics* **12**, e1005835 (2016). https://doi.org/10.1371/journal.pgen.1005835

28 Zhang, J. *et al.* Role of Protein Phosphatase1 Regulatory Subunit3 in Mediating the Abscisic Acid Response *Plant Physiology* **184**, 1317-1332 (2020). https://doi.org/10.1104/pp.20.01018

29 Hose, E., Clarkson, D. T., Steudle, E., Schreiber, L. & Hartung, W. The exodermis: a variable apoplastic barrier. *Journal of Experimental Botany* **52**, 2245-2264 (2001). https://doi.org/10.1093/jexbot/52.365.2245

30 Shiono, K. *et al.* RCN1/OsABCG5, an ATP-binding cassette (ABC) transporter, is required for hypodermal suberization of roots in rice (Oryza sativa). *The Plant Journal* **80**, 40-51 (2014). https://doi.org/10.1111/tpj.12614

31 Cantó-Pastor, A. *et al.* A suberized exodermis is required for tomato drought tolerance. *Nature Plants* **10**, 118-130 (2024). https://doi.org/10.1038/s41477-023-01567-x

32 Salas-González, I. *et al.* Coordination between microbiota and root endodermis supports plant mineral nutrient homeostasis. *Science* **371**, eabd0695 (2021). https://doi.org/10.1126/science.abd0695

33 Calvo-Polanco, M. *et al.* Physiological roles of Casparian strips and suberin in the transport of water and solutes. *New Phytologist* **232**, 2295-2307 (2021). https://doi.org/10.1111/nph.17765

34 Pascut, F. C. *et al.* Non-invasive hydrodynamic imaging in plant roots at cellular resolution. *Nature Communications* **12**, 4682 (2021). https://doi.org/10.1038/s41467-021-24913-z

35 Su, Y. *et al.* The evolutionary innovation of root suberin lamellae contributed to the rise of seed plants. *Nature Plants* **9**, 1968-1977 (2023). https://doi.org/10.1038/s41477-023-01555-1

36 Zhang, B. *et al.* Small peptide signaling via OsCIF1/2 mediates Casparian strip formation at the root endodermal and nonendodermal cell layers in rice. *The Plant Cell* **36**, 383-403 (2023). https://doi.org/10.1093/plcell/koad269

37 Lu, H. P. *et al.* An ABA-serotonin module regulates root suberization and salinity tolerance. *New Phytologist* **236**, 958-973 (2022). https://doi.org/10.1111/nph.18397

38 Feng, T. *et al.* Natural variation in root suberization is associated with local environment in Arabidopsis thaliana. *New Phytologist* **236**, 385-398 (2022). https://doi.org/https://doi.org/10.1111/nph.18341

39 Bouain, N. *et al.* Systems genomics approaches provide new insights into Arabidopsis thaliana root growth regulation under combinatorial mineral nutrient limitation. *PLOS Genetics* **15**, e1008392 (2019). https://doi.org/10.1371/journal.pgen.1008392

40 Ristova, D., Giovannetti, M., Metesch, K. & Busch, W. Natural genetic variation shapes root system responses to phytohormones in Arabidopsis. *The Plant Journal* **96**, 468-481 (2018). https://doi.org/https://doi.org/10.1111/tpj.14034

41 Alonso-Blanco, C. *et al.* 1,135 Genomes Reveal the Global Pattern of Polymorphism in Arabidopsis thaliana. *Cell* **166**, 481-491 (2016). https://doi.org/http://dx.doi.org/10.1016/j.cell.2016.05.063

42 Kover, P. X. *et al.* A Multiparent Advanced Generation Inter-Cross to Fine-Map Quantitative Traits in Arabidopsis thaliana. *PLOS Genetics* **5**, e1000551 (2009). https://doi.org/10.1371/journal.pgen.1000551

43 Nelson, B. K., Cai, X. & Nebenführ, A. A multicolored set of in vivo organelle markers for co-localization studies in Arabidopsis and other plants. *The Plant Journal* **51**, 1126-1136 (2007). https://doi.org/https://doi.org/10.1111/j.1365-313X.2007.03212.x

44 Lin, R. & Wang, H. Arabidopsis FHY3/FAR1 Gene Family and Distinct Roles of Its Members in Light Control of Arabidopsis Development. *Plant Physiology* **136**, 4010-4022 (2004). https://doi.org/10.1104/pp.104.052191

45 Liu, Y. *et al.* Type one protein phosphatases (TOPPs) contribute to the plant defense response in Arabidopsis. *Journal of Integrative Plant Biology* **62**, 360-377 (2020). https://doi.org/https://doi.org/10.1111/jipb.12845

46 Franck, C. M. *et al.* The Protein Phosphatases ATUNIS1 and ATUNIS2 Regulate Cell Wall Integrity in Tip-Growing Cells. *The Plant Cell* **30**, 1906-1923 (2018). https://doi.org/10.1105/tpc.18.00284

47 Fauser, F., Schiml, S. & Puchta, H. Both CRISPR/Cas-based nucleases and nickases can be used efficiently for genome engineering in rabidopsis thaliana. *The Plant Journal* **79**, 348-359 (2014). https://doi.org/https://doi.org/10.1111/tpj.12554

48 Ursache, R., Fujita, S., Dénervaud Tendon, V. & Geldner, N. Combined fluorescent seed selection and multiplex CRISPR/Cas9 assembly for fast generation of multiple Arabidopsis mutants. *Plant Methods* **17**, 111 (2021). https://doi.org/10.1186/s13007-021-00811-9

49 Geldner, N. *et al.* Rapid, combinatorial analysis of membrane compartments in intact plants with a multicolor marker set. *The Plant Journal* **59**, 169-178 (2009). https://doi.org/10.1111/j.1365-313X.2009.03851.x

50 Vermeer, J. E. M. *et al.* A Spatial Accommodation by Neighboring Cells Is Required for Organ Initiation in Arabidopsis. *Science* **343**, 178-183 (2014).

51 Mylle, E., Codreanu, M.-C., Boruc, J. & Russinova, E. Emission spectra profiling of fluorescent proteins in living plant cells. *Plant Methods* **9**, 10 (2013). https://doi.org/10.1186/1746-4811-9-10

52 Stöckle, D. *et al.* Microtubule-based perception of mechanical conflicts controls plant organ morphogenesis. *Sci Adv* **8**, eabm4974 (2022). https://doi.org/10.1126/sciadv.abm4974

53 Kalmbach, L. *et al.* Putative pectate lyase PLL12 and callose deposition through polar CALS7 are necessary for long-distance phloem transport in Arabidopsis. *Current Biology* **33**, 926-939.e929 (2023). https://doi.org/https://doi.org/10.1016/j.cub.2023.01.038

54 Siligato, R. *et al.* MultiSite Gateway-Compatible Cell Type-Specific Gene-Inducible System for Plants. *Plant Physiology* **170**, 627-641 (2016).

55 Clough, S. J. & Bent, A. F. Floral dip: a simplified method forAgrobacterium-mediated transformation ofArabidopsis thaliana. *The Plant Journal* **16**, 735-743 (1998). https://doi.org/10.1046/j.1365-313x.1998.00343.x

56 Shimada, T. L., Shimada, T. & Hara-Nishimura, I. A rapid and non-destructive screenable marker, FAST, for identifying transformed seeds of Arabidopsis thaliana. *The Plant Journal* **61**, 519-528 (2010).

57 Schindelin, J. *et al.* Fiji: an open-source platform for biological-image analysis. *Nature Methods* **9**, 676-682 (2012). https://doi.org/10.1038/nmeth.2019

58 Ferrero-Serrano, Á. & Assmann, S. M. Phenotypic and genome-wide association with the local environment of Arabidopsis. *Nature Ecology & Evolution* **3**, 274-285 (2019). https://doi.org/10.1038/s41559-018-0754-5

59 Naseer, S. *et al.* Casparian strip diffusion barrier in Arabidopsis is made of a lignin polymer without suberin. *Proceedings of the National Academy of Sciences* **109**, 10101-10106 (2012).

60 Berhin, A. *et al.* The Root Cap Cuticle: A Cell Wall Structure for Seedling Establishment and Lateral Root Formation. *Cell* **176**, 1367-1378.e1368 (2019). https://doi.org/10.1016/j.cell.2019.01.005

61 Horton, M. W. *et al.* Genome-wide patterns of genetic variation in worldwide Arabidopsis thaliana accessions from the RegMap panel. *Nature Genetics* **44**, 212-216 (2012). https://doi.org/http://www.nature.com/ng/journal/v44/n2/abs/ng.1042.html#supplementary-information

62 Madeira, F. *et al.* The EMBL-EBI Job Dispatcher sequence analysis tools framework in 2024. *Nucleic Acids Research* **52**, W521-W525 (2024). https://doi.org/10.1093/nar/gkae241

63 Livak, K. J. & Schmittgen, T. D. Analysis of relative gene expression data using real-time quantitative PCR and the 2(-Delta Delta C(T)) Method. *Methods (San Diego, Calif.)* **25**, 402-408 (2001). https://doi.org/10.1006/meth.2001.1262

64 Julkowska, M. M. *et al.* MVApp-Multivariate Analysis Application for Streamlined Data Analysis and Curation. *Plant Physiology* **180**, 1261-1276 (2019). https://doi.org/10.1104/pp.19.00235

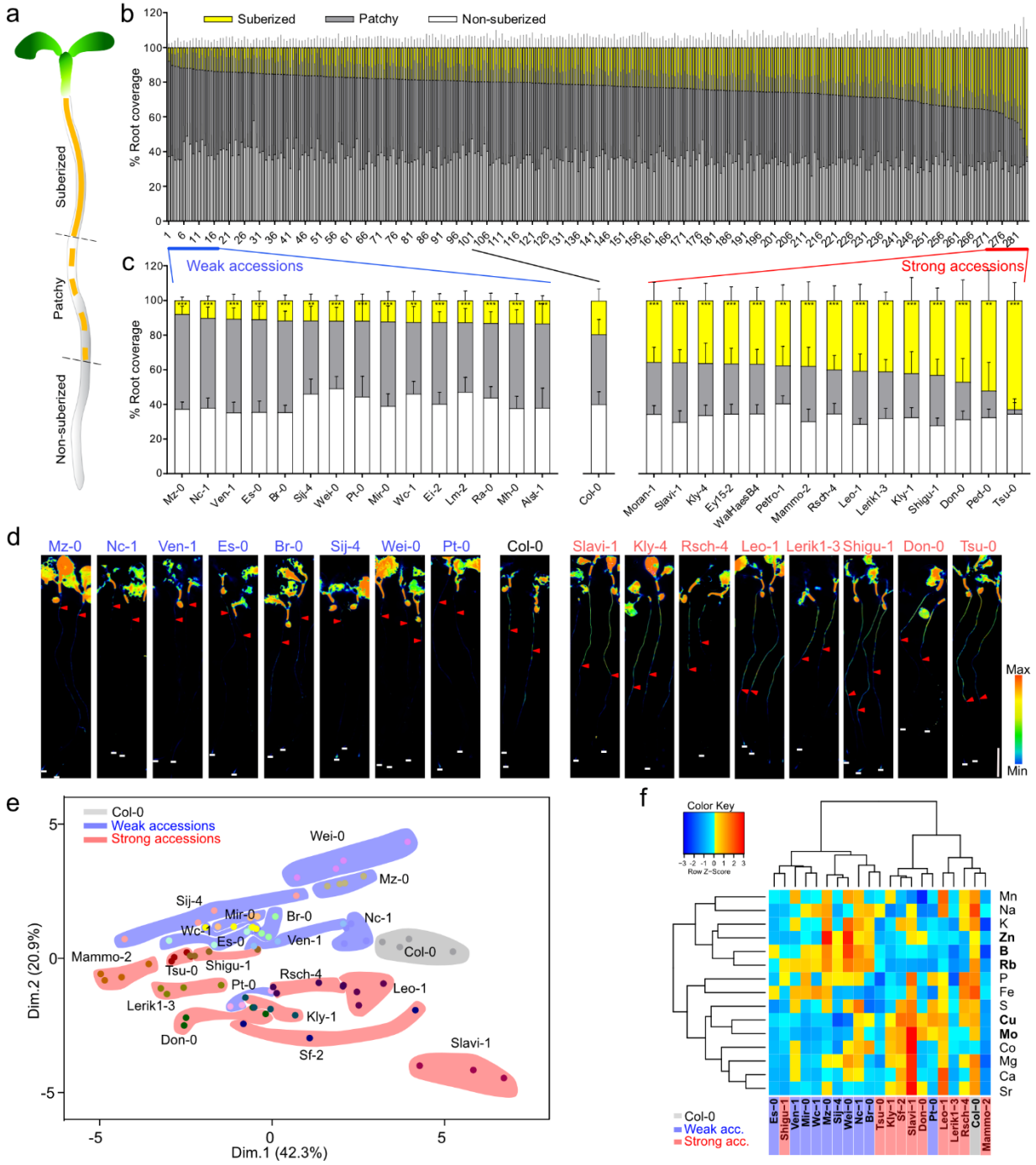

Fig. 1 | Natural variation in suberin deposition among Arabidopsis accessions. a, Schematic view of the three zones of suberization in roots. **b**, Quantification of suberin deposition in 4-day-old roots of 284 Arabidopsis accessions using Fluorol Yellow staining. Accessions are sorted by the percentage of suberized zone. Data are presented as stacked columns showing the mean percentage of each suberization zone + s.d., $n \geq 10$. Numeric values are provided in Supplementary Table 1. **c**, Comparison of suberin deposition in Col-0 and selected accessions representing the extremes (weak and strong) of the distribution shown in (**b**). Statistical differences in the suberized zone were assessed by one-way ANOVA followed by Dunnett's test and are presented for the comparison to Col-0 (**$P < 0.01$, ***$P < 0.001$). **d**, Whole-mount images of Fluorol Yellow-stained roots from selected extreme accessions. Red arrows indicate the onset of the suberized zone; white lines mark the root tip. Scale bar, 2 mm. **e**, Principal component analysis (PCA) of ionomic profiles in Col-0 and 20 extreme accessions. Accessions with weak and strong suberization are indicated with blue and red areas respectively (hand drawn). $n = 4$. **f**, Hierarchical clustering of ionomic profiles from the same set of extreme accessions. The 5 elements contributing most to the clustering are highlighted in bold. Data for (e-f) are available in Supplementary Table 3.

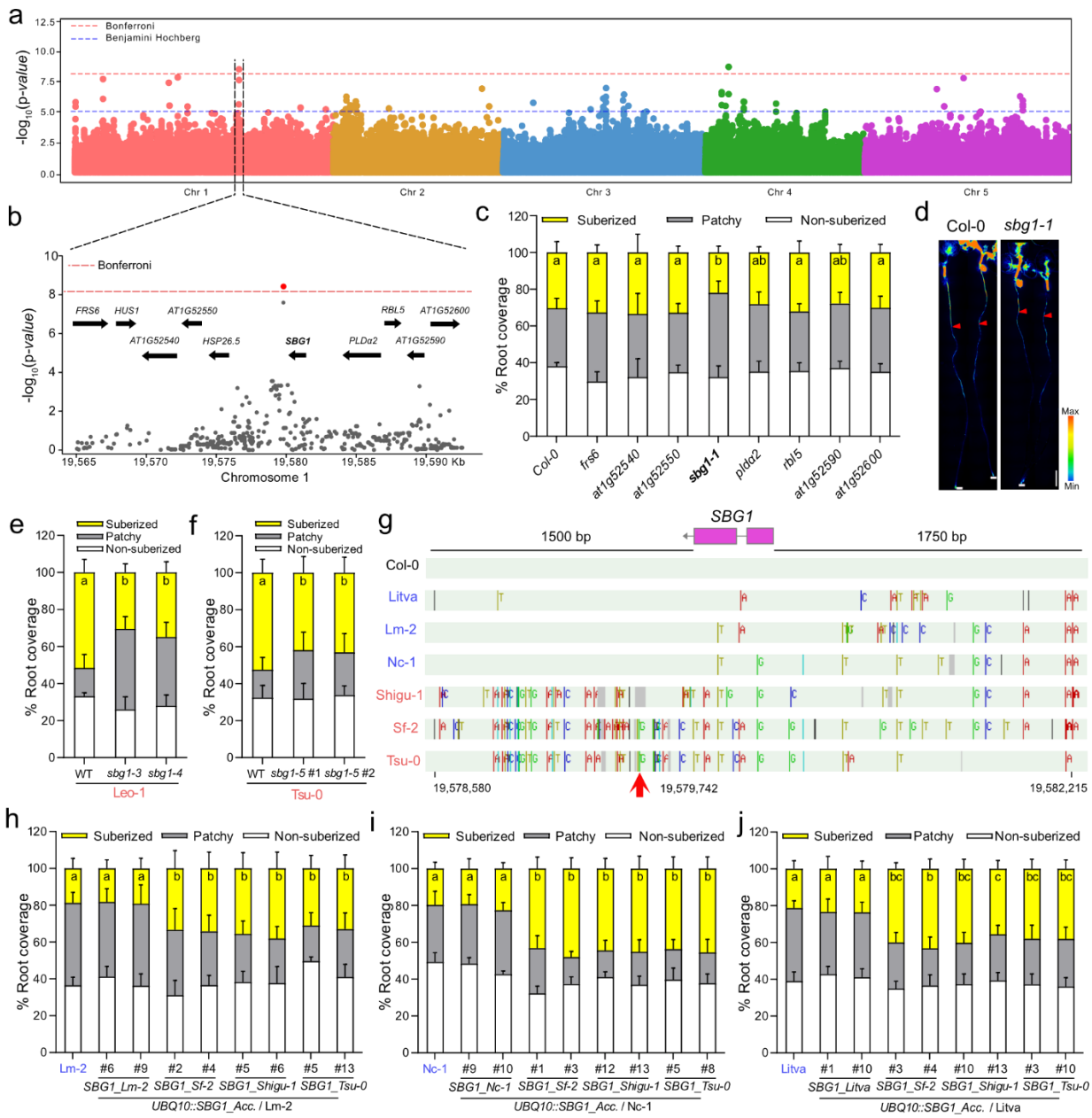

Fig. 2 | Identification of *SBG1* as a genetic determinant of suberin variations. a, Manhattan plot of GWAS for suberin variations across 265 accessions. Horizontal dashed lines indicate significant thresholds after multiple testing correction: red for Bonferroni and blue for Benjamini–Hochberg (FDR = 10%). **b**, SNPs and annotated genes surrounding the *SBG1* genomic region. Each dot represents a SNP, with the top SNP (19,579,742 bp) highlighted in red. **c**, Suberin deposition pattern in T-DNA insertion lines for candidate genes shown in (**b**). Data are presented as stacked columns showing the mean percentage of each suberization zone + s.d., $n = 10$. One-way ANOVA followed by a Tukey's test was used to assess significance for the suberized zone; different letters indicate significant differences between genotypes ($P < 0.05$). d, Whole-mount images of Fluorol Yellow-stained roots from Col-0 and sbg1-1 shown in (c). Red arrows indicate the onset of suberized zone; white lines mark the root tip. Scale bar, 1 mm. **e**,**f**, Suberin deposition pattern in *sbg1* mutants generated in Leo-1 (**e**) and Tsu-0 (**f**) backgrounds. Data are presented as in (**c**), $n = 10$. One-way ANOVA followed by a Tukey's test was used to test significance in the suberized zone ($P < 0.05$). **g**, SNP profiles in the *SBG1* genomic region across 3 *T* and 3 *G* allele accessions. The top SNP from GWAs is marked with a red arrow. SNP data were obtained from the 1001 Genomes dataset. **h**-**j**, Suberin deposition pattern in transgenic lines expressing *SBG1* under the *UBQ10* promoter in the background of Lm-2 (**h**), Nc-1 (**i**) and Litva (**j**). *SBG1* genomic sequence including 1.5 kb downstream of the stop codon was derived from Lm-2, Nc-1, Litva, Sf-2, Shigu-1 or Tsu-0 as indicated. Two independent lines were analyzed per construct. Data are presented as in (**c**). One-way ANOVA followed by a Tukey's test was used to determine significance in the suberized zone ($P < 0.05$).

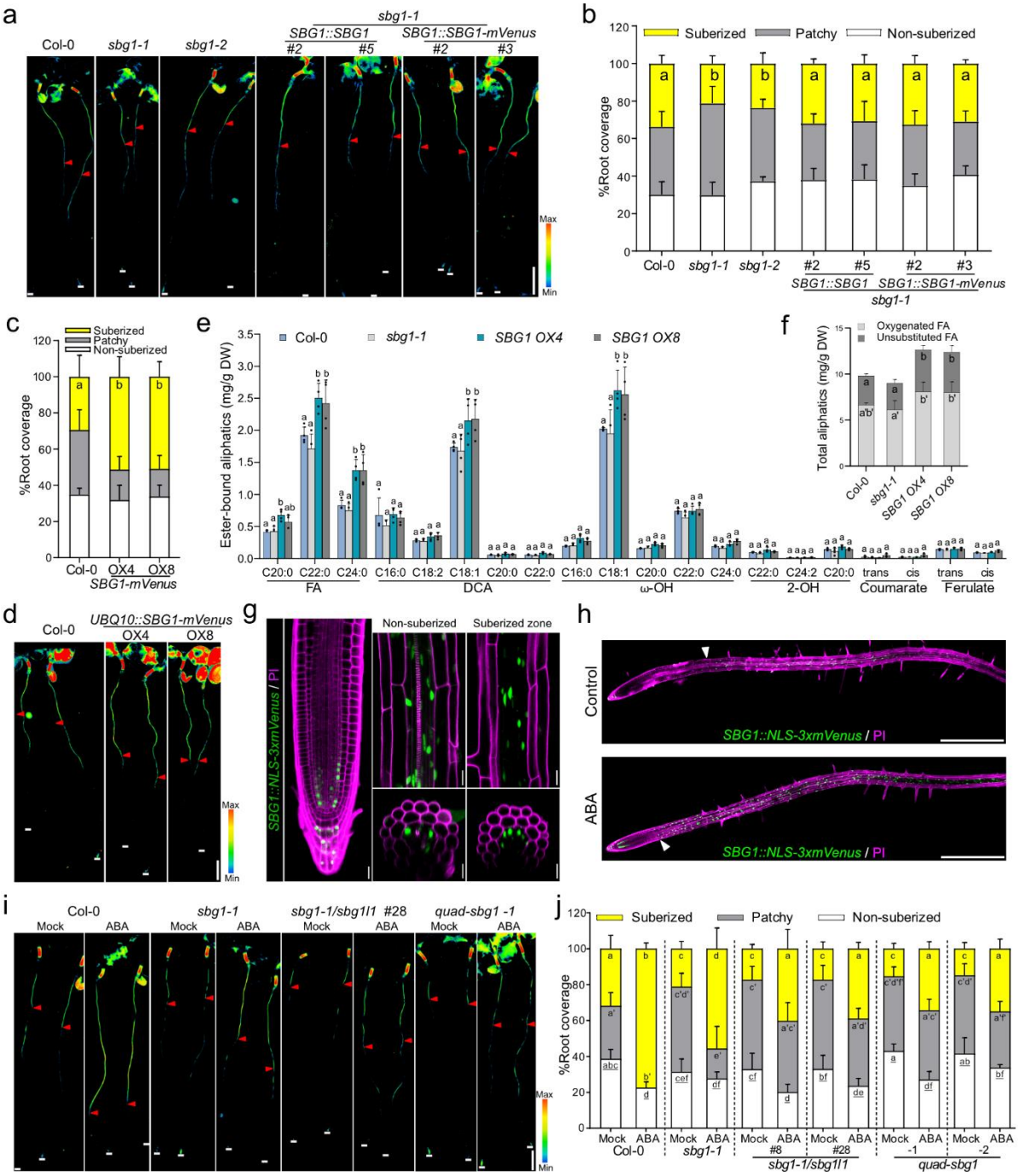

Fig. 3 | *SBG1* regulates suberization. a,**b**, Whole-mount images of Fluorol Yellow-stained roots (**a**) and suberin deposition pattern (**b**) in *sbg1* mutants and complemented lines. Red arrows indicate the onset of suberized zone; white lines mark the root tip. Scale bar, 1 mm. Data are presented as stacked columns showing the mean percentage of each suberization zone + s.d., n = 10. One-way ANOVA followed by a Tukey's test was used to assess significance for the suberized zone; different letters indicate significant differences between genotypes (P < 0.05). **c**,**d**, Whole-mount images (**c**) and quantification (**d**) of suberin deposition in transgenic lines expressing *SBG1-mVenus* under the *UBQ10* promoter. Data are presented as in (**a**,**b**). **e**,**f**, Quantification of ester-bound aliphatic and aromatic suberin monomers in 5-day-old roots.

FA, fatty acid; DCA, dicarboxylic fatty acid; ω-OH, ω-hydroxy fatty acid; DW, dry weight. Data are shown as histograms with individual values overlaid, s.d., $n = 4$. Two-way ANOVA followed by a Tukey's test was used to assess significance for each suberin monomer, oxygenated and unsubstituted FA; different letters indicate significant differences between genotypes ($P < 0.05$). **g**, Confocal images of *SBG1::NLS-3xmVenus* line showing mVenus signal (green) combined with PI staining (magenta) to highlight cell walls. In the non-suberized and suberized root zones, mVenus signal was projected in 3D. Cross-section views were generated by re-slicing Z-stacks. Scale bar, 20 µm. **h**, Confocal images of *SBG1::NLS-3xmVenus* lines treated with or without 1 µM ABA for 18h. mVenus signal is shown in green and PI in magenta. White arrows indicate the onset of mVenus signal after the division zone. Scale bar, 500 µm. **i**,**j**, Whole-mount images (**i**) and suberin deposition pattern (**j**) in *sbg1-1* and high-order *sbg1l* mutants under control (mock) or 1 µM ABA treatment for 18h. 4-day-old seedlings were transferred to either ½ MS plates or ½ MS plate + ABA. Data are presented as in (**a,b**). Apostrophes and underlines indicate different statistical comparisons.

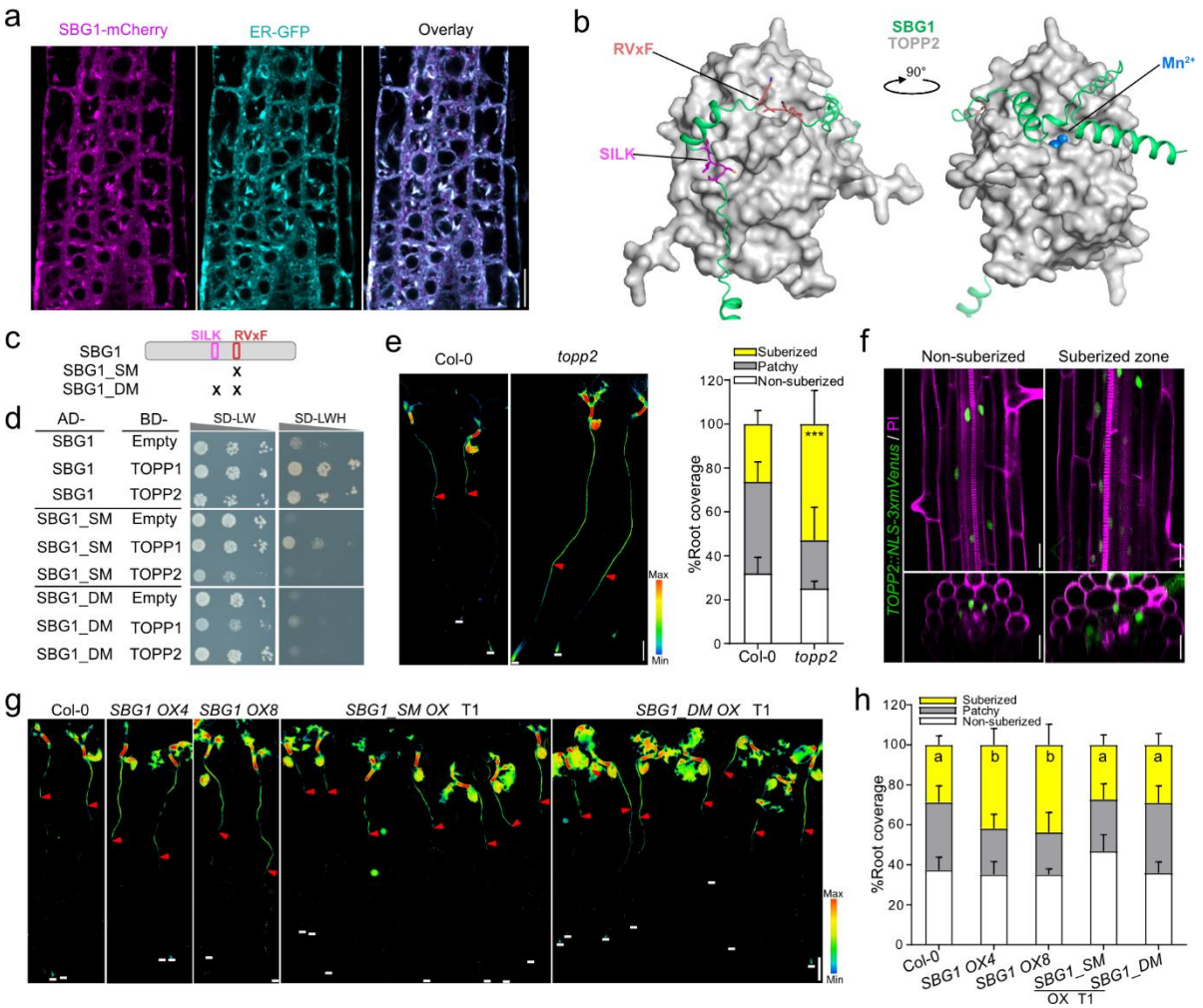

Fig. 4 | SBG1 regulates suberization through its interaction with TOPPs. **a**, Confocal images showing colocalization of SBG1-mCherry (magenta) with ER-GFP (cyan). Individual channels and merged images are shown Scale bar, 50 µm. **b**, Predicted AlphaFold3 structure of SBG1 in complex with TOPP2. The side chains of the SILK and RVxF motifs in SBG1 and two Mn^{2+} ions in the catalytic domain of TOPP2 are highlighted. **c**, Schematic representation of mutations in the SBG1 binding motifs. SM denotes mutation in the RVxF motif, and DM denotes combined mutations in both the SILK and RVxF motifs. Mutation sites are marked with an "X". **d**, Yeast two-hybrid assay showing interactions between WT or mutated forms of SBG1 (SM and DM) and TOPP1 or TOPP2. Drop test started with OD600 of 0.1 followed by 10 times dilutions. **e**, Whole-mount images of Fluorol Yellow-stained roots and corresponding suberin deposition pattern in *topp2*. Red arrows indicate the onset of the suberized zone; white lines mark the root tip. Scale bar, 1 mm. Data are presented as stacked columns showing the mean percentage of each suberization zone + s.d., n = 11. Student's t-test was used to assess significance between genotypes in the suberized zone (***P < 0.001). **f**, Confocal images of *TOPP2::NLS-3xmVenus* in roots showing mVenus signal (green) overlaid with PI staining (magenta) to visualize cell walls. mVenus signal was projected in 3D. Cross-section views were generated by re-slicing Z-stacks. Scale bar, 50 µm. **g**,**h**, Whole-mount images (**g**) and suberin deposition pattern (**h**) in T1 overexpression lines expressing *SBG1_SM* and *SBG1_DM* compared to WT *SBG1* (*SBG1 OX4* and *8*). Data are presented as in (**e**). One-way ANOVA followed by Tukey's test was used to assess significance in the suberized zone; different letters indicate significant differences between genotypes (P < 0.05). n = 11 for Col-0 and *SBG1 OX4*/8, n = 20 for *SBG1_SM OX* (independent T1 lines), and n = 16 for *SBG1_DM OX* (independent T1 lines).